# Structural and Biological Comparative Studies on M(II)-Complexes of Hydrazone-*s*-Triazine Ligand Bearing Pyridyl Arm

**Mezna Saleh Altowyan [1], Ayman El-Faham [2,3], MennaAllah Hassan [3], Assem Barakat [4], Matti Haukka [5], Morsy A. M. Abu-Youssef [3], Saied M. Soliman [3,*] and Amal Yousri [3,*]**

[1] Department of Chemistry, College of Science, Princess Nourah bint Abdulrahman University, P.O. Box 84428, Riyadh 11671, Saudi Arabia; msaltowyan@pnu.edu.sa
[2] Department of Clinical Sciences, College of Medicine, Dar Al Uloom University, P.O. Box 45142, Riyadh 11512, Saudi Arabia; ayman.a@dau.edu.sa or ayman.elfaham@alexu.edu.eg or aymanel_faham@hotmail.com
[3] Department of Chemistry, Faculty of Science, Alexandria University, P.O. Box 426, Ibrahimia, Alexandria 21321, Egypt; mennaallahhassanelsayed@gmail.com (M.H.); morsy5@alexu.edu.eg (M.A.M.A.-Y.)
[4] Department of Chemistry, College of Science, King Saud University, P.O. Box 2455, Riyadh 11451, Saudi Arabia; ambarakat@ksu.edu.sa
[5] Department of Chemistry, University of Jyväskylä, P.O. Box 35, FI-40014 Jyväskylä, Finland; matti.o.haukka@jyu.fi
* Correspondence: saied1soliman@yahoo.com or saeed.soliman@alexu.edu.eg (S.M.S.); amal.yousri@alexu.edu.eg or amalyousri@yahoo.com (A.Y.)

.

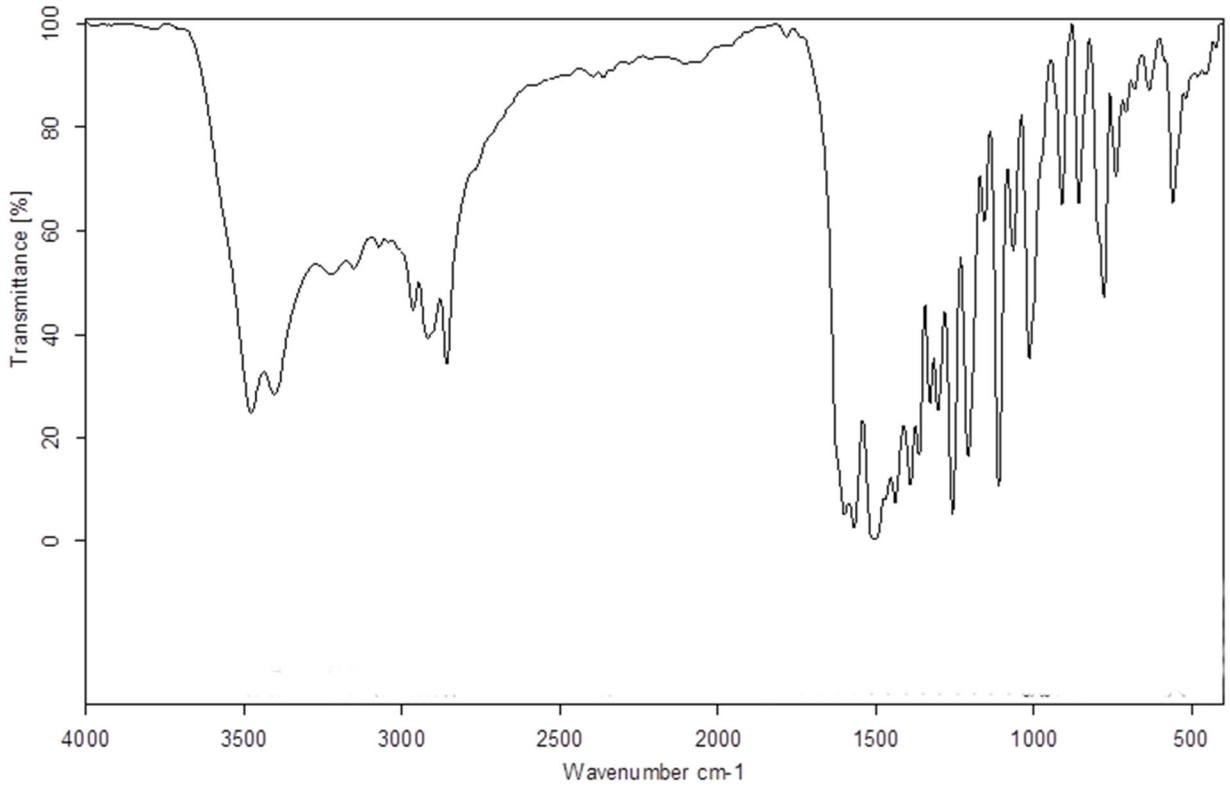



**Figure S1**. The FTIR spectra of the [Co(**$^{BM}$PyTr**)$Cl_2$]·$H_2O$.

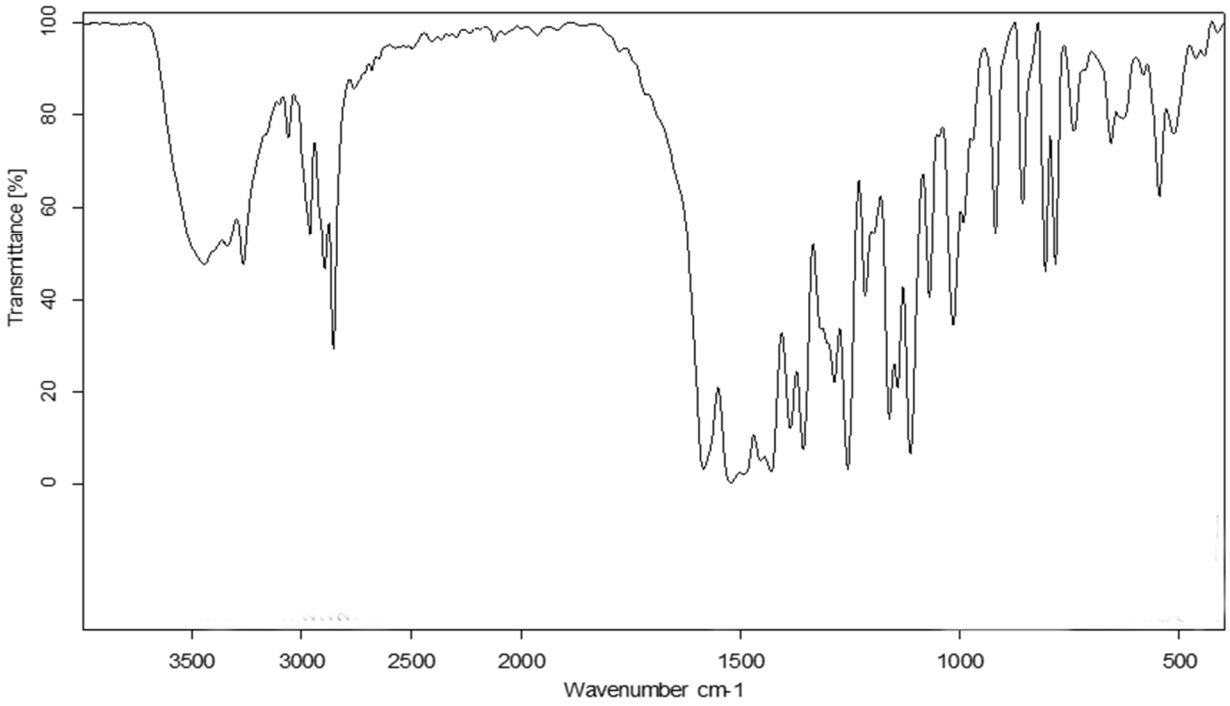



**Figure S2**. The FTIR spectra of the free ligand (**$^{BM}$PyTr**).

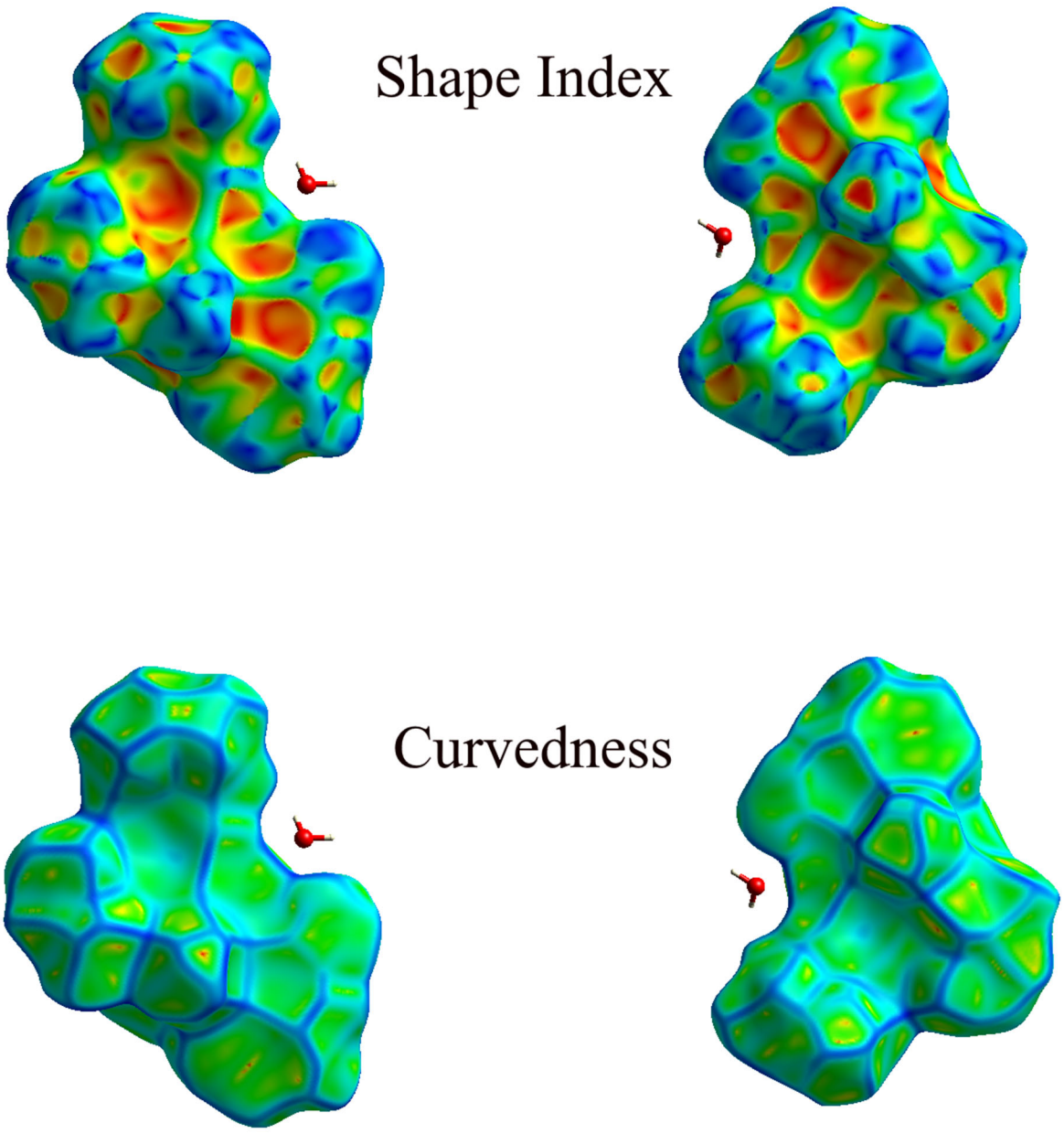



**Figure S3**. The curvedness and shape index surfaces for the [Co(**$^{BM}$PyTr**)$Cl_2$]·$H_2O$ complex.

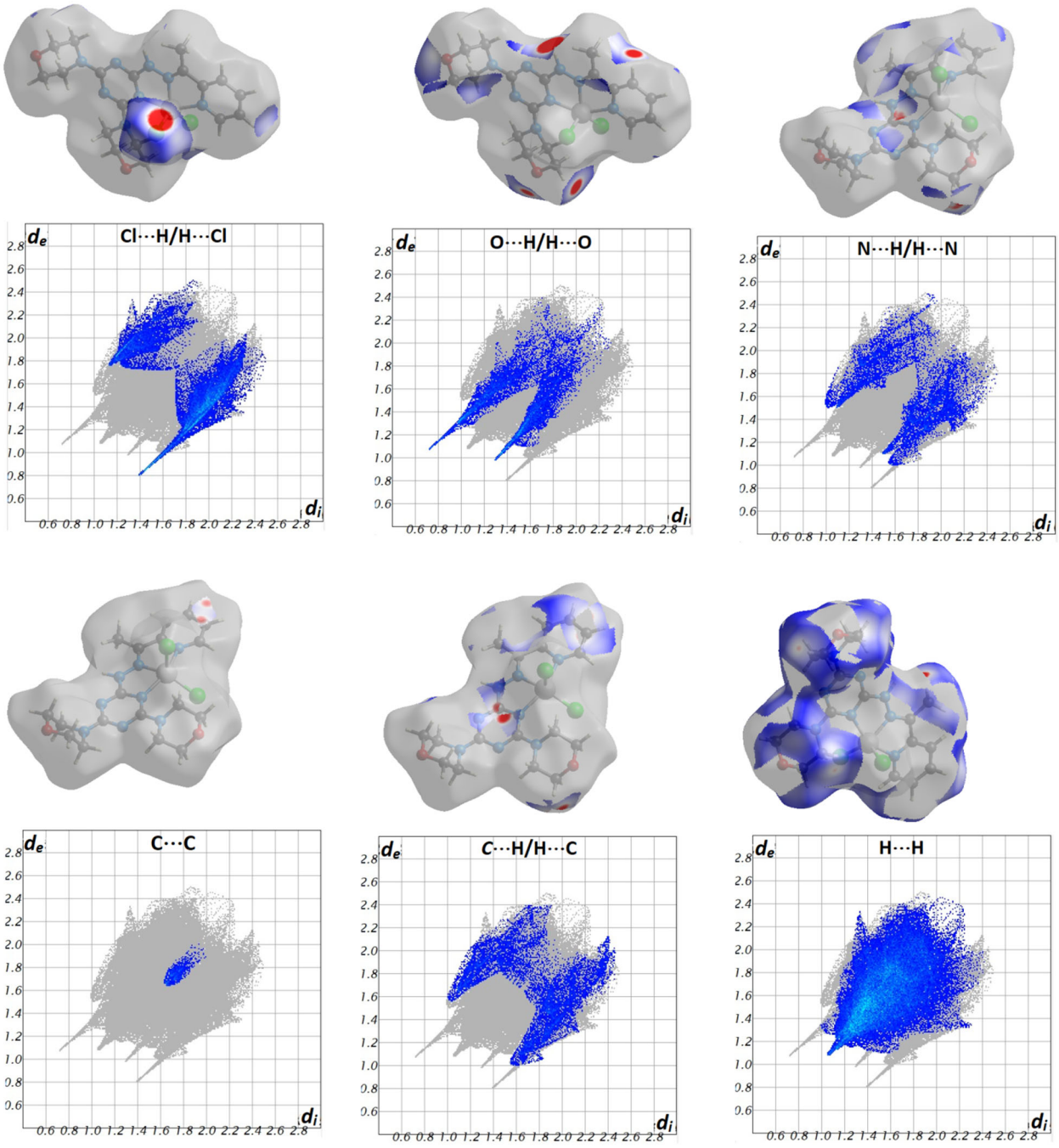



**Figure S4**. The fingerprint plots for the unit with letter B in the atom numbering for [Co(**$^{BM}$PyTr**)$Cl_2$]·$H_2O$ complex.

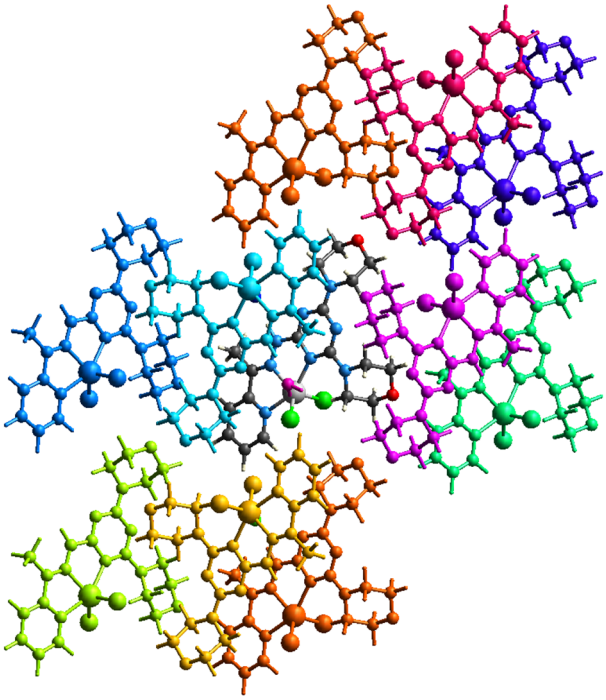


**Figure S5**. Visualization of molecular interactions within a cluster with a radius of 3.8 Å between the central molecule under investigation and its neighboring molecules, viewed along the *a*-axis.

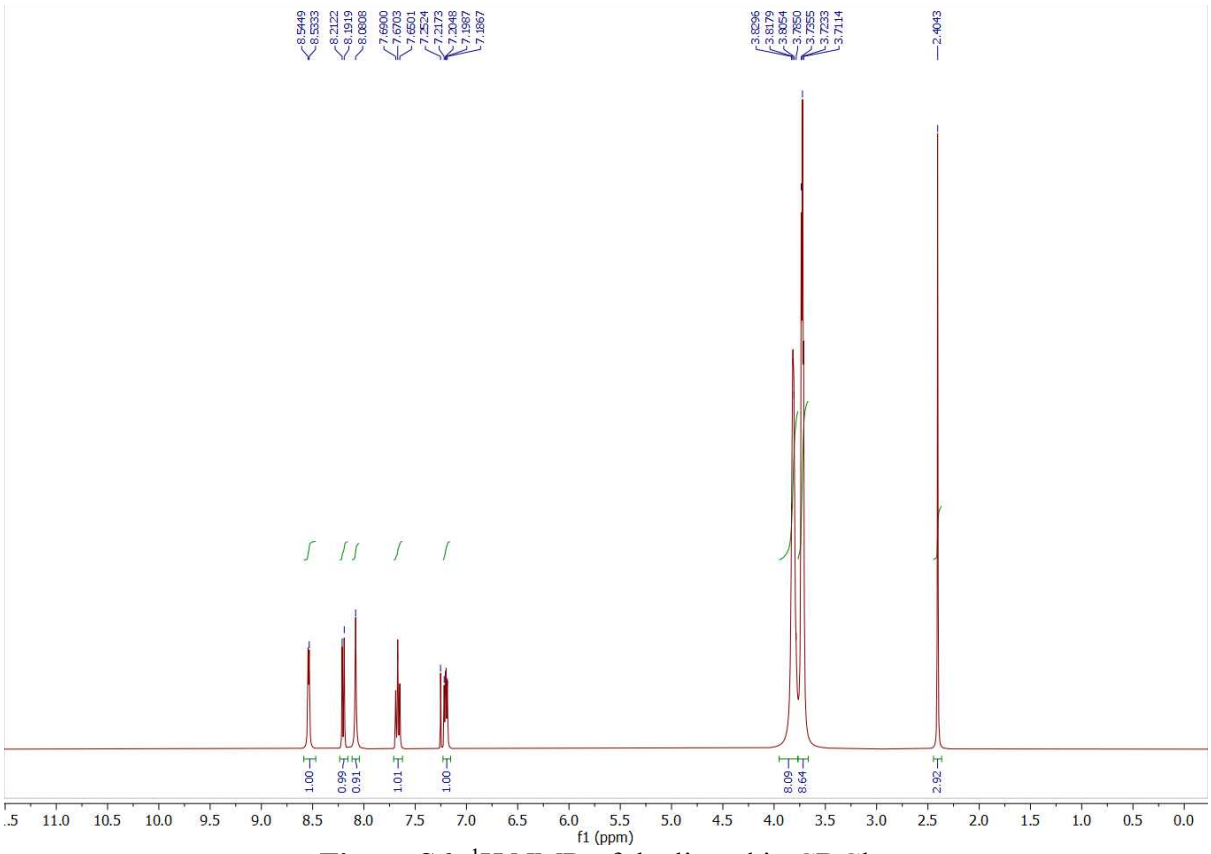



**Figure S6**. $^{1}H$ NMR of the ligand in $CDCl_3$.

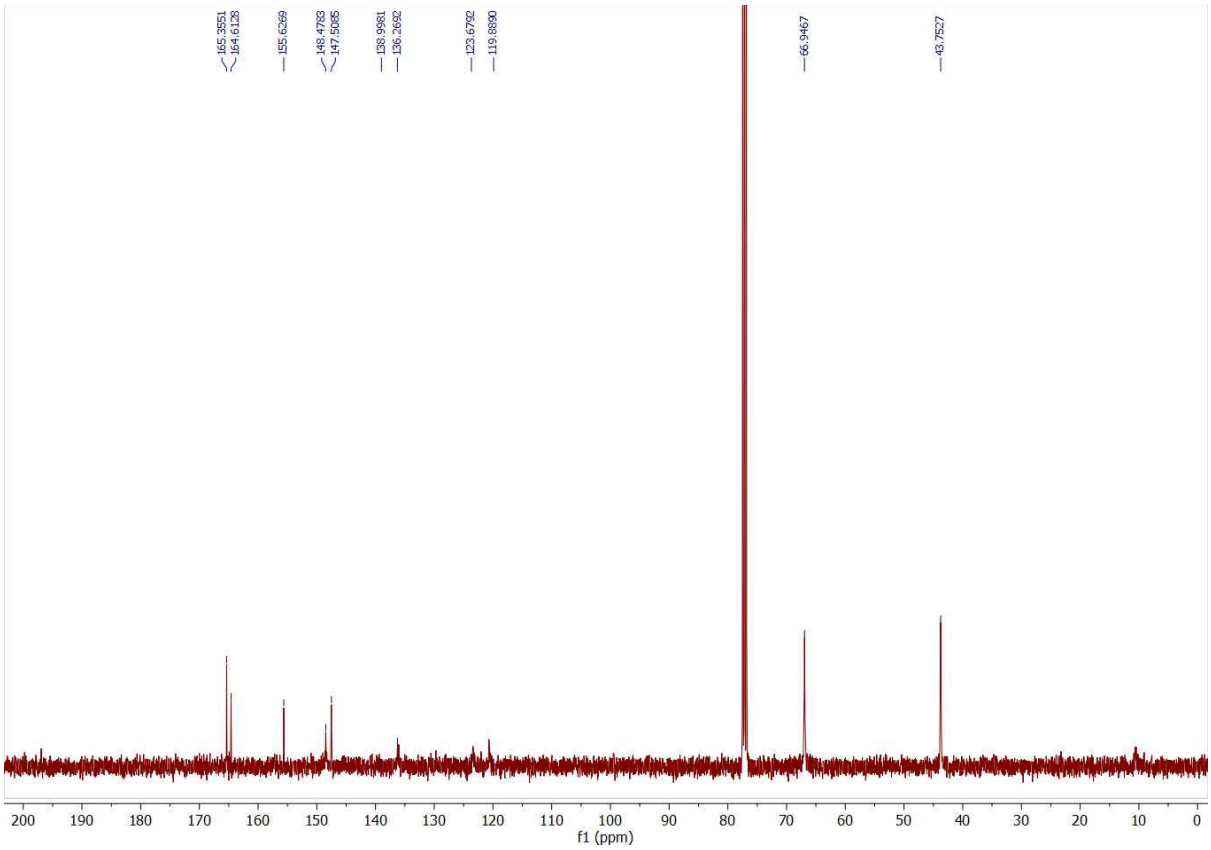



**Figure S7**. $^{13}C$ NMR of the ligand in $CDCl_3$.

**Table S1.** The short intermolecular interactions in the [Co(**$^{BM}$PyTr**)$Cl_2$]·$H_2O$.

| **contact** | **Distance (Å)** | **contact** | **Distance (Å)** |
|---|---|---|---|
| O1···H17A | 2.509 | C4···H14B | 2.727 |
| O2···H4B | 2.321 | C9···H16C | 2.608 |
| O3···H3 | 1.768 | C10···H16C | 2.751 |
| O3···H7B | 2.374 | C1B···H11C | 2.742 |
| O4···H3B | 1.804 | C8B···H16B | 2.705 |
| O4···H7BC | 2.289 | C10B···H16B | 2.588 |
| O1B···H17D | 2.289 | C1···C2 | 3.329 |
| O2B···H4 | 2.376 | C1B···C2B | 3.319 |
| N7···H7C | 2.571 | Cl1···H3D | 2.281 |
| N7···H16C | 2.534 | Cl2···H1 | 2.838 |
| N4B···H16B | 2.585 | Cl2···H3C | 2.180 |
| N7B···H7BA | 2.612 | Cl1B···H4C | 2.294 |
| H3A···H13C | 2.147 | Cl2B···H4A | 2.205 |
| H14A···H18C | 2.154 | | |

**Table S2.** Different interaction energies of the molecular pairs in kJ/mol for the [Co(**$^{BM}$PyTr**)$Cl_2$]·$H_2O$.

| N | Symop | R | Electron Density | $E_{ele}$ | $E_{pol}$ | $E_{dis}$ | $E_{rep}$ | $E_{tot}$ |
|---|---|---|---|---|---|---|---|---|
| 1 | -x, -y, -z | 12.05 | HF/3-21G | 0.0 | -16.1 | 0.0 | 0.0 | -10.5 |
| 1 | x, y, z | 11.86 | HF/3-21G | -8.4 | -6.3 | -20.5 | 8.8 | -24.0 |
| 0 | -x, -y, -z | 10.46 | HF/3-21G | -29.8 | -20.5 | -20.6 | 25.0 | -42.0 |
| 1 | -x, -y, -z | 7.77 | HF/3-21G | -21.4 | -22.1 | -61.9 | 25.1 | -71.6 |
| 1 | - | 8.47 | HF/3-21G | 0.0 | -16.1 | 0.0 | 0.0 | -10.5 |
| 1 | - | 4.83 | HF/3-21G | 0.0 | -16.1 | 0.0 | 0.0 | -10.5 |
| 0 | -x, -y, -z | 5.23 | HF/3-21G | -50.7 | -30.6 | -124.0 | 71.5 | -125.2 |
| 0 | - | 11.13 | HF/3-21G | -8.4 | -6.3 | -20.5 | 8.8 | -24.0 |
| 0 | - | 4.91 | HF/3-21G | -8.4 | -6.3 | -20.5 | 8.8 | -24.0 |
| 0 | - | 15.64 | HF/3-21G | -21.4 | -22.1 | -61.9 | 25.1 | -71.6 |
| 0 | - | 8.10 | HF/3-21G | 0.0 | -20.4 | 0.0 | 0.0 | -13.3 |
| 0 | - | 4.25 | HF/3-21G | -29.8 | -20.5 | -20.6 | 25.0 | -42.0 |
| 0 | - | 15.52 | HF/3-21G | -50.7 | -30.6 | -124.0 | 71.5 | -125.2 |

Interaction Energies (kJ/mol)

R is the distance between molecular centroids (mean atomic position) in Å.

Total energies, only reported for two benchmarked energy models, are the sum of the four energy components, scaled appropriately.

Scale factors for benchmarked energy models [63].

| Energy Model | $k_{ele}$ | $k_{pol}$ | $k_{disp}$ | $k_{rep}$ |
|---|---|---|---|---|
| CE-HF ... HF/3-21G electron densities | 1.019 | 0.651 | 0.901 | 0.811 |
| CE-B3LYP ... B3LYP/6-31G(d,p) electron densities | 1.057 | 0.740 | 0.871 | 0.618 |

**Table S3**. Evaluation of anticancer activity against HCT-116 cell line for **$^{BM}$PyTr** [48].

| Sample conc. (µM) | Viability % | Inhibitory % | S.D. (±)[a] |
|---|---|---|---|
| 1300.6 | 6.37 | 93.63 | 0.59 |
| 650.3 | 14.62 | 85.38 | 0.64 |
| 325.1 | 31.79 | 68.21 | 1.37 |
| 162.6 | 47.28 | 52.72 | 2.94 |
| 81.3 | 79.46 | 20.54 | 2.32 |
| 40.6 | 95.72 | 4.28 | 0.56 |
| 20.3 | 98.64 | 1.36 | 0.48 |
| 10.1 | 100 | 0 | |
| 5.2 | 100 | 0 | |
| 2.6 | 100 | 0 | |
| 0.0 | 100 | 0 | |

[a] Standard deviation

**Table S4**. Evaluation of anticancer activity against HCT-116 cell line for **1**.

| Sample conc. (µM) | Viability % | Inhibitory % | S.D. (±)[a] |
|---|---|---|---|
| 939.3 | 11.85 | 88.15 | 0.93 |
| 469.7 | 29.47 | 70.53 | 1.61 |
| 234.8 | 48.21 | 51.79 | 2.47 |
| 117.4 | 67.54 | 32.46 | 3.02 |
| 58.7 | 89.03 | 10.97 | 1.69 |
| 29.3 | 97.16 | 2.84 | 0.48 |
| 14.7 | 100 | 0 | |
| 7.3 | 100 | 0 | |
| 3.8 | 100 | 0 | |
| 1.9 | 100 | 0 | |
| 0.0 | 100 | 0 | |

[a] Standard deviation

**Table S5**. Evaluation of anticancer activity against HCT-116 cell line for **2** [48].

| Sample conc. (µM) | Viability % | Inhibitory % | S.D. (±)[a] |
|---|---|---|---|
| 979.9 | 4.23 | 95.77 | 0.51 |
| 489.9 | 11.76 | 88.24 | 0.82 |
| 245.0 | 24.98 | 75.02 | 1.74 |
| 122.5 | 35.43 | 64.57 | 2.91 |
| 61.2 | 49.86 | 50.14 | 3.22 |
| 30.6 | 78.02 | 21.98 | 2.94 |
| 15.3 | 93.27 | 6.73 | 0.55 |
| 7.6 | 98.43 | 1.57 | 0.19 |
| 3.9 | 100 | 0 | |
| 2.0 | 100 | 0 | |
| 0.0 | 100 | 0 | |

[a] Standard deviation

**Table S6**. Evaluation of anticancer activity against HCT-116 cell line for **3** [48].

| Sample conc. (µM) | Viability % | Inhibitory % | S.D. (±)[a] |
|---|---|---|---|
| 931.3 | 2.39 | 97.61 | 0.27 |
| 465.6 | 5.87 | 94.13 | 0.31 |
| 232.8 | 11.42 | 88.58 | 0.65 |
| 116.4 | 23.96 | 76.04 | 0.42 |
| 58.2 | 34.65 | 65.35 | 1.23 |
| 29.1 | 48.12 | 51.88 | 1.96 |
| 14.5 | 68.41 | 31.59 | 2.07 |
| 7.3 | 84.07 | 15.93 | 1.29 |
| 3.7 | 95.34 | 4.66 | 0.62 |
| 1.9 | 99.26 | 0.74 | 0.48 |
| 0.0 | 100 | 0 | |

[a] Standard deviation

**Table S7**. Evaluation of anticancer activity against HCT-116 cell line for **4** [50].

| Sample conc. (µM) | Viability % | Inhibitory % | S.D. (±)[a] |
|---|---|---|---|
| 871.3 | 3.79 | 96.21 | 0.28 |
| 435.7 | 6.95 | 93.05 | 0.40 |
| 217.8 | 15.43 | 84.57 | 1.38 |
| 108.9 | 29.61 | 70.39 | 2.49 |
| 54.5 | 48.16 | 51.84 | 3.62 |
| 27.2 | 65.39 | 34.61 | 3.05 |
| 13.6 | 73.22 | 26.78 | 1.46 |
| 6.8 | 81.45 | 18.55 | 1.69 |
| 3.5 | 89.21 | 10.79 | 0.78 |
| 1.7 | 94.36 | 5.64 | 0.73 |
| 0.0 | 100 | 0 | |

[a] Standard deviation

**Table S8**. Evaluation of anticancer activity against HCT-116 cell line for **5** [50].

| Sample conc. (µM) | Viability % | Inhibitory % | S.D. (±)[a] |
|---|---|---|---|
| 883.4 | 4.31 | 95.69 | 0.23 |
| 441.7 | 8.72 | 91.28 | 0.81 |
| 220.9 | 19.65 | 80.35 | 0.65 |
| 110.4 | 37.18 | 62.82 | 1.87 |
| 55.2 | 56.03 | 43.97 | 2.28 |
| 27.6 | 78.92 | 21.08 | 1.48 |
| 13.8 | 86.16 | 13.84 | 1.27 |
| 6.9 | 92.74 | 7.26 | 0.85 |
| 3.5 | 98.56 | 1.44 | 0.21 |
| 1.8 | 100 | 0 | |
| 0.0 | 100 | 0 | |

[a] Standard deviation

**Table S9**. Evaluation of anticancer activity against A-549 cell line for **$^{BM}$PyTr** [48].

| Sample conc. (µM) | Viability % | Inhibitory % | S.D. (±)[a] |
|---|---|---|---|
| 1300.6 | 5.92 | 94.08 | 0.46 |
| 650.3 | 12.97 | 87.03 | 0.39 |
| 325.1 | 28.65 | 71.35 | 0.71 |
| 162.6 | 44.93 | 55.07 | 2.19 |
| 81.3 | 68.72 | 31.28 | 2.46 |
| 40.6 | 90.61 | 9.39 | 1.37 |
| 20.3 | 98.74 | 1.26 | 0.28 |
| 10.1 | 100 | 0 | |
| 5.2 | 100 | 0 | |
| 2.6 | 100 | 0 | |
| 0.0 | 100 | 0 | |

[a] Standard deviation

**Table S10**. Evaluation of anticancer activity against A-549 cell line for **1**.

| Sample conc. (µM) | Viability % | Inhibitory % | S.D. (±)[a] |
|---|---|---|---|
| 939.3 | 8.74 | 91.26 | 0.92 |
| 469.7 | 20.36 | 79.64 | 1.78 |
| 234.8 | 39.75 | 60.25 | 2.61 |
| 117.4 | 51.36 | 48.64 | 3.48 |
| 58.7 | 74.12 | 25.88 | 1.42 |
| 29.3 | 83.41 | 16.59 | 0.37 |
| 14.7 | 92.78 | 7.22 | 0.54 |
| 7.3 | 98.46 | 1.54 | 0.12 |
| 3.8 | 100 | 0 | |
| 1.9 | 100 | 0 | |
| 0.0 | 100 | 0 | |

[a] Standard deviation

**Table S11**. Evaluation of anticancer activity against A-549 cell line for **2** [48].

| Sample conc. (µM) | Viability % | Inhibitory % | S.D. (±)[a] |
|---|---|---|---|
| 979.9 | 6.81 | 93.19 | 0.57 |
| 489.9 | 15.34 | 84.66 | 0.88 |
| 245.0 | 29.49 | 70.51 | 1.37 |
| 122.5 | 48.17 | 51.83 | 2.69 |
| 61.2 | 79.04 | 20.96 | 2.42 |
| 30.6 | 94.86 | 5.14 | 1.08 |
| 15.3 | 99.08 | 0.92 | 0.64 |
| 7.6 | 100 | 0 | |
| 3.9 | 100 | 0 | |
| 2.0 | 100 | 0 | |
| 0.0 | 100 | 0 | |

[a] Standard deviation

**Table S12**. Evaluation of anticancer activity against A-549 cell line for **3** [48].

| Sample conc. (µM) | Viability % | Inhibitory % | S.D. (±)[a] |
|---|---|---|---|
| 931.3 | 3.64 | 96.36 | 0.28 |
| 465.6 | 7.52 | 92.48 | 0.44 |
| 232.8 | 13.89 | 86.11 | 0.63 |
| 116.4 | 24.73 | 75.27 | 1.25 |
| 58.2 | 38.17 | 61.83 | 2.09 |
| 29.1 | 57.49 | 42.51 | 2.17 |
| 14.5 | 82.75 | 17.25 | 1.31 |
| 7.3 | 94.02 | 5.98 | 0.46 |
| 3.7 | 98.74 | 1.26 | 0.62 |
| 1.9 | 100 | 0 | |
| 0.0 | 100 | 0 | |

[a] Standard deviation

**Table S13**. Evaluation of anticancer activity against A-549 cell line for **4** [50].

| Sample conc. (µM) | Viability % | Inhibitory % | S.D. (±)[a] |
|---|---|---|---|
| 871.3 | 4.27 | 95.73 | 0.33 |
| 435.7 | 8.78 | 91.22 | 0.77 |
| 217.8 | 17.64 | 82.36 | 1.25 |
| 108.9 | 35.07 | 64.93 | 1.59 |
| 54.5 | 52.38 | 47.62 | 2.20 |
| 27.2 | 71.42 | 28.58 | 0.59 |
| 13.6 | 85.09 | 14.91 | 1.13 |
| 6.8 | 88.65 | 11.35 | 0.54 |
| 3.5 | 97.42 | 2.58 | 0.28 |
| 1.7 | 99.23 | 0.77 | 0.26 |
| 0 | 100 | 0 | |

[a] Standard deviation

**Table S14**. Evaluation of anticancer activity against A-549 cell line for **5** [50].

| Sample conc. (µM) | Viability % | Inhibitory % | S.D. (±)[a] |
|---|---|---|---|
| 883.4 | 5.63 | 94.37 | 0.27 |
| 441.7 | 12.59 | 87.41 | 1.29 |
| 220.9 | 24.16 | 75.84 | 1.63 |
| 110.4 | 43.89 | 56.11 | 2.56 |
| 55.2 | 69.51 | 30.49 | 2.35 |
| 27.6 | 84.17 | 15.83 | 1.93 |
| 13.8 | 91.59 | 8.41 | 0.65 |
| 6.9 | 98.03 | 1.97 | 0.37 |
| 3.5 | 100 | 0 | |
| 1.8 | 100 | 0 | |
| 0.0 | 100 | 0 | |

[a] Standard deviation

**Table S15**. Evaluation of anticancer activity against A-549 cell line for $CoCl_2$ [75].

| Sample conc. (µM) | Viability % | Inhibitory % | S.D. (±)[a] |
|---|---|---|---|
| 2101.5 | 67.13 | 32.87 | 16.60 |
| 1050.7 | 95.2 | 4.8 | 5.97 |
| 525.4 | 99.74 | 0.26 | 2.19 |
| 262.7 | 100 | 0 | |
| 131.3 | 100 | 0 | |
| 65.6 | 100 | 0 | |
| 32.8 | 100 | 0 | |
| 16.4 | 100 | 0 | |
| 0.0 | 100 | 0 | |

***Materials and physical characterizations***

All chemicals and solvents were purchased from Sigma-Aldrich Chemical Company Inc. (St. Louis, MO, USA) and were utilized without additional purification. The FTIR spectra were obtained using a Bruker Tensor 37 FTIR instrument, Bruker, Germany, employing the KBr disc method and recording the spectra in the range of 4000–400 $cm^{-1}$. A PerkinElmer 2400 Elemental Analyzer was employed for CHN analysis (PerkinElmer Inc., Waltham, MA, USA). The metal content was determined using a Shimadzu atomic absorption spectrophotometer (AA7000 series, Shimadzu, Ltd., Kyoto, Japan). The UV-Vis electronic spectra were recorded in ethanol using Pg instruments T80+ spectrophotometer (Alma Park, Wibtoft Leicstershire, UK).

**Method S1.** Synthesis of ligand (**$^{BM}$PyTr**)

A solution of 2-acetylpyridine (2 mmol, 242 mg), drop of acetic acid and *s*-triazine-hydrazine derivative (2 mmol, 563 mg) in EtOH (20 ml) were mixed and heated under reflux overnight (TLC 2% MeOH/$CHCl_3$ then 50:50 EtOAc/n-hexane). The product was precipitated after evaporation into 1/3 of the solvent and kept overnight, then the reaction mixture was filtered off, subsequently washed with small amount of EtOH to afford the final product (**$^{BM}$PyTr**) as a white precipitate.

**Ligand (**$^{BM}$**PyTr):** m.p: 230°C; IR (KBr, $cm^{-1}$): 3442 ν (N–H), 2962, 2895, 2855 ν(C–H), 1606, 1584 ν(C=N), 1523, 1492 ν(C=C), 1256 ν(C–N). $^1$H NMR (400 MHz, $CDCl_3$) δ 8.54 (d, *J* = 4.6 Hz, 1H), 8.20 (d, *J* = 8.1 Hz, 1H), 8.08 (s, 1H), 7.67 (t, *J* = 8.0 Hz, 1H), 7.20 (dd, *J* = 7.3, 4.9 Hz, 1H), 3.81 (q, *J* = 8.2, 6.4 Hz, 8H), 3.72 (t, *J* = 4.8 Hz, 8H), 2.40 (s, 3H) ppm (**Figure S6**). $^{13}$C NMR (101 MHz, $CDCl_3$) δ 165.36, 164.61, 155.63, 148.48, 147.51, 139.00, 136.27, 123.68, 119.89, 66.95, 43.75 ppm (**Figure S7**).

**Method S2. Crystal structure determination**

The crystal of [Co($^{BM}$PyTr)$Cl_2$]*$H_2O$ was immersed in cryo-oil, mounted in a loop, and measured at a temperature of 120 K. The X-ray diffraction data was collected on a Rigaku Oxford Diffraction XtaLAB Synergy R diffractometer using Cu Kα radiation. The CrysAlisPro [76] software package was used for cell refinement and data reduction. A multi-scan absorption correction (CrysAlisPro [76]) was applied to the intensities before the structure solution. The structure was solved by the intrinsic phasing (SHELXT [77]) method. Structural refinement was carried out using SHELXL [78] software with SHELXLE [79] graphical user interface. The asymmetric unit contains two crystallographically independent cobalt molecules. The NH and $H_2O$ hydrogen atoms, involved in the hydrogen bonding network, were located from the difference Fourier map and refined isotropically. All other hydrogen atoms were positioned geometrically and constrained to ride on their parent atoms, with C-H = 0.95 -0.99 Å and Uiso = 1.2-1.5·Ueq(parent atom).

**Method S3. Energy framework analysis protocol**

The energy framework study is a valuable method used to analyze the topology of molecular interactions within a crystal [63,64]. This technique involves calculating and comparing various energy components such as repulsion ($E_{rep}$), electrostatic ($E_{ele}$), dispersion ($E_{dis}$), polarization ($E_{pol}$), and total ($E_{tot}$) energy. These calculations are based on the anisotropy of the topology of pairwise intermolecular interaction energies. They encompass electrostatic energy, which deals with the forces between charged particles; polarization energy, which arises from the distortion of a molecule's electron cloud by nearby charge distributions; dispersive energy, which involves weak attractive forces resulting from temporary fluctuations in a molecule's electron distribution; and repulsive energy, which is the energy needed to overcome the forces preventing two molecules from interacting. The total interaction energy of the molecule is the sum of these different interaction energies [64,65], as represented in the following formula:

$$E_{tot} = E_{ele} + E_{pol} + E_{dis} + E_{rep}$$

In the analysis of the title compound, the Crystal Explorer program [69,70] was utilized to determine the energy framework. The computational approach involved generating new wave functions. The energy framework is represented by cylinders, with the thickness of the cylinders indicating the strength of interactions. The thickness is directly proportional to the energy magnitude, providing valuable insights into the stabilization of the crystal packing [64,66]. The calculations were based on the HF/3-21G level of theory, and the software facilitated the calculation of interaction energies for a 3.8 Å cluster around a single molecule, using scale factors consistent with established values [63,67,78]. The resulting three-dimensional energy frameworks were visualized to emphasize neighboring molecules within a 3.8 Å radius from the reference molecule (**Figure S5**). The data presented in **Table S2** for the energy frameworks illustrate the contributions of different components, including $E_{ele}$, $E_{pol}$, $E_{dis}$, $E_{rep}$, and $E_{tot}$, to various intermolecular interactions in the compound. Additionally, the calculations involved symmetry operations to construct molecular wave functions and estimate electron densities, enabling the calculation of electrostatic, polarization, dispersion, and exchange-repulsion energy components. This approach provided valuable insights into the organization of the tested compounds within their crystal structures. Also, **Table S2** not only provides an energy breakdown but also details such as the color-coding scheme corresponding to molecular

interactions at specific Cartesian coordinates. It includes components of the interaction energies (E), the number of pairs of interacting molecules with the reference molecule (N), the centroid-to-centroid distance between the reference molecule and interacting molecules (R), and the associated rotational symmetry operations (symmetry). These details are crucial for lattice energy calculations [72-74].

**Method S4. Evaluation of anticancer activity [85]**

*Cell line Propagation*

The cells were obtained from the American Type Culture Collection (ATCC, Rockville, MD) and were propagated in Dulbecco's modified Eagle's medium (DMEM) supplemented with 10% heat-inactivated fetal bovine serum, 1% L-glutamine, HEPES buffer and 50µg/mL Gentamycin. Cells were maintained at 37ºC in a humidified atmosphere with 5% $CO_2$ and were subcultured two times a week.

*Cytotoxicity evaluation using viability assay*

For cytotoxicity assay, the cells were seeded in 96-well plate at a cell concentration of $1\times10^4$ cells per well in 100µl of growth medium. Fresh medium containing different concentrations of the test sample was added after 24 h of seeding. Serial two-fold dilutions of the tested chemical compound were added to confluent cell monolayers dispensed into 96-well, flat-bottomed microtiter plates (Falcon, NJ, USA) using a multichannel pipette. The microtiter plates were incubated at 37ºC in a humidified incubator with 5% $CO_2$ for a period of 24 h. Three wells were used for each concentration of the test sample. Control cells were incubated without test sample and with or without DMSO. The little percentage of DMSO present in the wells (maximal 0.1%) was found not to affect the experiment. After incubation of the cells for at 37°C, for 24 h, the viable cells yield was determined by the MTT test. Briefly, the media was removed from the 96 well plate and replaced with 100 µL of fresh culture DMEM medium without phenol red then 10 µL of the 12 mM MTT stock solution (5 mg of MTT in 1 mL of PBS) to each well including the untreated controls. The 96-well plates were then incubated at 37°C and 5% $CO_2$ for 4 h. An 85 µL aliquot of the media was removed from the wells, and 50 µL of DMSO was added to each well and mixed thoroughly with the pipette and incubated at 37°C for 10 min. Then, the optical density was measured at 590 nm with the microplate reader (SunRise, TECAN, Inc, USA) to determine the number of viable cells and the percentage of viability was calculated as [(ODt/ODc)]x100% where ODt is the mean optical density of wells treated with the tested sample and ODc is the mean optical density of untreated cells. The relation between surviving cells and drug concentration is plotted to get the survival curve of each tumor cell line after treatment with the specified compound. The 50% inhibitory concentration ($IC_{50}$), the concentration required to cause toxic effects in 50% of intact cells, was estimated from graphic

plots of the dose response curve for each concentration using Graphpad Prism software (San Diego, CA. USA).

**Method S5. Evaluation of antimicrobial activity [86]**

*a) Tested pathogenic microbes*

The antimicrobial activity was evaluated against two gram-positive bacteria ((*S. aureus* (ATCC 25923) and *B. subtilis* (RCMB015(1)NRR LB-543)), two gram-negatvie bacteria ((*E. coli* (ATCC 25922) and *P. vulgaris* (RCMB 004(1)ATCC 13315)) and two fungi ((*A. fumigatus* (RCMB 002008) and *C. albicans* (RCMB 005003(1) ATCC 10231)). Gentamycin was used as standard antibacterial agent. The samples maintained in Brain heart infusion (BHI) at 20ºC; 300 mL of each stock-culture was added to 3 mL of BHI broth. Overnight cultures were kept for 24 h at 37 ºC ± 1ºC and the purity of cultures was checked after 24 h of incubation. After 24 h of incubation, bacterial suspension was diluted with sterile physiological solution, for the diffusion and indirect bioautographic tests, to 108 CFU/mL (turbidity = McFarland barium sulfate standard 0.5). In case of fungi *A. fumigatus* (RCMB 002008) and *C. albicans* (RCMB 005003(1) ATCC 10231), the used medium in antagonistic activity against tested fungi is Potato Dextrose Agar, where Ketoconazole was used standard antifungal agent.

*b) Agar well diffusion method*

Synthetic compound was prepared at concentration 10 mg/mL dissolved in DMSO as stock solutions. Preparation of sterilized Mueller Hinton agar plates seeded with tested pathogenic bacteria occurred. The wells are done by sterilized cork borer in size 6 mm and hence 100 µL of the synthetic compound was poured in each well comparably with DMSO as control. The plates were incubated at 37°C for 24-48 h (for bacteria) and at 28°C for 48 h (for fungi). After incubation period; antimicrobial activity was determined by inhibition zones.

*C) Minimum Inhibitory Concentration (MIC)*

Different dilutions of the compound are inoculated with tested pathogenic microbes. After incubation period of 96-well microplate, the results are measured using microplate reader. To determine at what level the MIC endpoint is established; subculture of test samples at different concentrations occurred in nutrient agar plates.

**References**

63. Turner, M.J.; Thomas, S.P.; Shi, M.W.; Jayatilaka, D.; Spackman, M.A. Energy frameworks: insights into interaction anisotropy and the mechanical properties of molecular crystals. *Chem. Commun.* **2015***, 51*, 3735-3738.

64. Bakheit, A.H.; Attwa, M.W.; Kadi, A.A.; Alkahtani, H.M. Structural Analysis and Reactivity Insights of (E)-Bromo-4-((4-((1-(4-chlorophenyl) ethylidene) amino)-5-phenyl-4H-1,2,4-triazol-3-yl) thio)-5-((2-isopropylcyclohexyl) oxy) Furan-2(5H)-one: A combined approach using single-crystal X-ray diffraction, Hirshfeld surface analysis, and conceptual density functional theory. *Crystals* **2023***, 13*, 1313.

65. Turner, M.J.; Grabowsky, S.; Jayatilaka, D.; Spackman, M.A. Accurate and efficient model energies for exploring intermolecular interactions in molecular crystals. *J. Phys. Chem. Lett.* **2014***, 5,* 4249-4255.

66. Hajji, M.; Mtiraoui, H.; Amiri, N.; Msaddek, M.; Guerfel, T. Crystallographic and first-principles density functional theory study on the structure, noncovalent interactions, and chemical reactivity of 1,5-benzodiazepin-2-ones derivatives. *Int. J. Quantum Chem.* **2019***, 119,* e26000.

67. Abad, N.; Sallam, H.H.; Al-Ostoot, F.H.; Khamees, H.A.; Al-horaibi, S.A.; Khanum, S.A.; Madegowda, M.; El Hafi, M.; Mague, J.T.; Essassi, E.M. Synthesis, crystal structure, DFT calculations, Hirshfeld surface analysis, energy frameworks, molecular dynamics and docking studies of novel isoxazolequinoxaline derivative (IZQ) as anti-cancer drug. *J. Mol. Struct.* **2021***, 1232,* 130004.

68. Edwards, A.J.; Mackenzie, C.F.; Spackman, P.R.; Jayatilaka, D.; Spackman, M.A. Intermolecular interactions in molecular crystals: what's in a name? Farad. *Disc.* **2017***, 203,* 93-112.

72. Tan, S.L.; Jotani, M.M.; Tiekink, E.R. Utilizing Hirshfeld surface calculations, non-covalent interaction (NCI) plots and the calculation of interaction energies in the analysis of molecular packing. *Acta Cryst.* **2019***, E75*, 308-318.

73. Sreenatha, N.; Chakravarthy, A.J.; Suchithra, B.; Lakshminarayana, B.; Hariprasad, S.; Ganesha, D. Crystal, spectral characterization, molecular docking, Hirshfeld computational studies and 3D-energy framework analysis of a novel puckered compound (C14H15ClO): 2-Chloro-3-phenyl-5,5-dimethylcyclohex-2-en-1-one. *J. Mol. Struct.* **2020***, 1210*, 127979.

74. Guo, Z.A.; Xian, J.Y.; Rong, L.R.; Qin, H.; Jie, Z. Theoretical study of metal ion impact on geometric and electronic properties of terbutaline compounds. *Monatsh. Chem.* **2019***, 150*, 1355-1364.

75. Refaat, H.M.; Alotaibi, A.A.M.; Dege, N.; El-Faham, A.; Soliman, S.M. Co(II) complexes based on the bis-pyrazol-s-triazine pincer ligand: synthesis, X-ray structure studies, and cytotoxic evaluation. *Crystals* **2022**, 12, 741.

76. Rikagu Oxford Diffraction, CrysAlisPro, 2020, Rikagu Oxford Diffraction inc., Yarnton, Oxfordshire, England.

77. Sheldrick, G.M. SHELXT – Integrated space-group and crystal-structure determination *Acta Cryst.* **2015***, A71*, 3-8.

78. Sheldrick, G.M. Crystal structure refinement with SHELXL. *Acta Cryst.* **2015***, C71*, 3-8.

79. Hübschle, C.B.; Sheldrick, G.M.; Dittrich, B. ShelXle: A Qt graphical user interface for SHELXL. *J. Appl. Cryst.* **2011***, 44,* 1281-1284.

80. Spackman, M.A.; Jayatilaka, D. Hirshfeld surface analysis. *CrystEngComm* **2009***, 11*, 19-32.

81. Turner, M.; McKinnon, J.; Wolff S.; Grimwood, D.; Spackman, P.; Jayatilaka, D.; Spackman, M. CrystalExplorer17, University of Western Australia, 2017.

85. Mosmann, T. Rapid colorimetric assay for cellular growth and survival: application to proliferation and cytotoxicity assays. *J. Immunol. Methods* **1983***, 65*, 55-63.

86. Lu, P.L.; Liu, Y.C.; Toh, H.S.; Lee, Y.L.; Liu, Y.M.; Ho, C.M.; Huang, C.C.; Liu, C.E.; Ko, W.C.; Wang, J.H. Epidemiology and antimicrobial susceptibility profiles of Gram-negative bacteria causing urinary tract infections in the Asia-Pacific region: 2009–2010 results from the Study for Monitoring Antimicrobial Resistance Trends (SMART). *Int. J. Antimicrob. Agents* **2012***, 40*, S37-S43.